Radiative Heat Exchange Modeling Inside an Oven

Ashish Dhall and Ashim K. Datta
Dept. of Biological and Environmental Engineering, Cornell University, Ithaca, NY 14853

Kenneth E. Torrance
School of Mechanical and Aerospace Engineering, Cornell University, Ithaca, NY 14853

Marialuci F. Almeida
Dept. of Food Science, Cornell University, Ithaca, NY 14853

DOI 10.1002/aic.11903
Published online July 17, 2009 in Wiley InterScience (www.interscience.wiley.com).

The 3D nongray radiative heat exchange in a near-infrared commercial oven is modeled. The spectrum is divided into into four gray bands to model the narrow wavelength range in which the halogen heat source radiates, the wavelength dependence of the food surface emittance, and the absorption coefficient of the heat source cover glass. The model is used to estimate the heating of a cuboidal food sample for 1 min at different cyclic settings of a halogen radiant heat source. The model predictions agree with the experimental data, and capture the cover-glass and the food-surface temperature and heat flux histories very well. The band-wise distribution of energy absorption by the food reveals the separate contributions from the source and the oven walls. Comparison of the heating rates between the measured non-gray food-surface and the different gray food-surface emittance values establishes the necessity of the nongray treatment. © *2009 American Institute of Chemical Engineers*
AIChE J, 55: 2448–2460, 2009
Keywords: food, infrared, non-gray, heat flux, discrete ordinates

Introduction

The infrared heating of food in an oven is a classic process. More recently, infrared heating has been combined with other modes of heating such as microwave or forced hot air. Different regions of the infrared spectrum, such as the near-infrared (halogen), have been introduced.[1–5] The low penetration depth of infrared waves leads to rapid surface heating which has been exploited to produce effects such as the pre-drying of sheeted foods (chips, tortillas, etc.) and the surface browning of meat products (to seal the meat juice) that are not possible with other modes of heating. The exchange of radiation between an infrared source and the food inside an oven is a complex process. Surface properties of the food are an important factor in determining the amount of energy absorbed and these properties can vary with radiation wavelength. The radiation surface properties can also vary with food composition, temperature, and surface conditions. The complex radiation exchange process determines the temperature-time history and therefore the final quality of a heated food such as crust formation and color development.[6,7] A better understanding of the effects of various food and oven parameters on infrared heating should lead to improved optimization of this heating, contributing to better quality of infrared-heated food, novel uses of infrared energy in food processing, less energy usage, and

Correspondence concerning this article should be addressed to A. K. Datta at akd1@cornell.edu

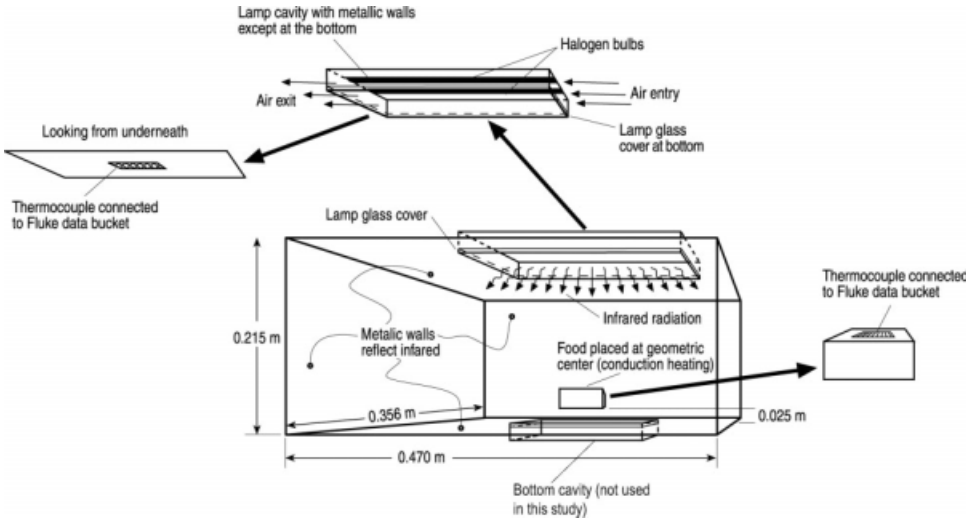

Figure 1. Schematic of the radiation dominant problem.

The geometry of the oven is rectangular, of size 0.470 m × 0.356 m ×0.215 m (volume 3.6×10^{-2} m^3). The food inside the oven is a potato slab of geometry 0.0470 m ×0.0356 m ×0.0215 m that has a volume 3.6×10^{-5} m^3. Food is placed at 2.5 cm above the geometric center of the oven's bottom surface and parallel, resting on a quartz glass tray.

increased automation of food processing through appropriate combinations of infrared with other modes of heating such as microwave.

Fundamentals-based analyses of the food heating process that allow for complexities such as the variation in radiative properties (i.e., reflection, absorption) and the effects of source wavelength do not exist, generally speaking.[8] Studies have been either qualitative or were very simple analyses of the radiative exchange assuming black or gray surfaces; complete radiative exchange analyses are complex and have not been performed.[9–15] Models of infrared exchange in nonfood applications such as computer graphics imaging, microelectronics, and paper and wood processing are more complete but do not include the combinations of geometry, radiative properties, and other physical parameters that typically describe food heating.[16–19]

The present study (1) develops a thermal radiative exchange model for a 3-D cavity that uses wavelength-dependent (nongray) radiative properties for the heat source, the oven and the food materials, and predicts the oven wall temperatures, food temperatures, and time-varying heat fluxes; (2) experimentally validates the predicted temperatures and heat fluxes; and (3) performs sensitivity analyses with the model for the input food and oven parameters. The article starts with a description of the problem, the governing equations, and the boundary conditions for thermal radiative exchange. Then, input parameters are discussed, followed by a description of experimental measurements. In the last two sections of the article, validation results and sensitivity analyses are presented.

Mathematical Model

The physical geometry is sketched in Figure 1. Radiative heat exchange occurs inside an oven (a 3-D enclosure) which has two halogen lamps in a top cavity and one halogen lamp in a bottom cavity (not used in this study). The food is placed inside the oven just above the floor.

The lamp cavities are covered by transparent glass plates. The halogen lamps emit infrared radiation with the spectrum shown in Figure 2. Most of the short wavelength radiation emitted by the lamps (~71%[20]) is transmitted by the cavity glass; the longer wavelength radiation as well as that emitted by the oven walls, is absorbed by the glass. The food surface properties can vary with wavelength. The lamp is cycled on-off by the heating control system. During this process, the lamp maintains its emission spectrum, while the heat flux magnitude changes with cycling. Thus, we model the lamp as an essentially constant temperature source with a time-varying heat flux. The emitted flux is assumed to originate

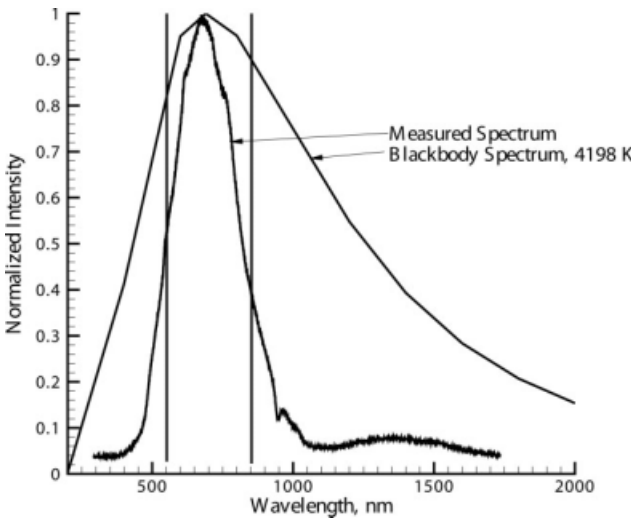

Figure 2. Radiation spectrum of the source with blackbody spectrum at 4198 K superimposed on it.

Band cuts at 550 nm and 850 nm also shown.

from two small heated strips in the top surface of the lamp cavity, as shown in Figure 1. The emitted radiant intensity is used with the radiative transport equation (RTE), and is coupled with the heat conduction equations for the food and air to solve for temperature.

Assumptions

Some of the major assumptions in developing the mathematical formulation include: (1) All surfaces are diffuse emitters and reflectors, with no directional dependence — the surface roughness of foods and the roughness and coatings on the oven surfaces are likely to support this assumption; (2) Problem is radiation dominant and natural convection effects are minor since the heating is only for a short time interval; (3) Food is a solid conductive body that is opaque to thermal radiation, i.e., all energy is absorbed at the surface. The penetration depth in the food for near infrared radiation has been reported to be small (close to 1.5 mm[21]), which justifies the opaque assumption.

Governing equation and boundary conditions for radiative heat exchange

Governing Equations. Radiation exchange inside the oven involves the heat source, food, oven walls, and glass cover plate on the source. The ambient air is taken as radiatively transparent (i.e., nonparticipating). The heat source, food, and walls participate only by surface emission and absorption. The glass cover plate absorbs and emits internally, and transmits overall. Within the cover plate, we must solve the radiative transport equation, RTE,[22,23] which is given by

$$\nabla.(I(\mathbf{r},\mathbf{s})\mathbf{s}) = -a(I(\mathbf{r},\mathbf{s}) + n^2 I_b(\mathbf{r})) \tag{1}$$

where I is the radiation intensity (beam energy per unit time and unit area normal to the beam, and per unit solid angle).

The RTE describes the variation of the radiation intensity, $I(\mathbf{r},\mathbf{s})$, at a location $\mathbf{r}$, in a direction $\mathbf{s}$, and at a specific wavelength λ. The blackbody intensity in the glass is denoted by $I_b(\mathbf{r})$. The two terms of the right side of (Eq. 1) account for absorption and emission, respectively, in the glass. The absorption coefficient and index of refraction of the glass are denoted by a and n. We neglect in- and out-scattering inside the glass in Eq. 1.

The ambient air is assumed to be radiatively transparent (i.e., non-absorbing, emitting, or scattering). Thus, a beam of radiant energy of intensity $I(\mathbf{s})$ leaving a surface is unattenuated as it passes through the air, and is constant (and conserved) until it strikes another surface. Absorption, emission and reflection can occur at the solid surfaces, and, as noted, absorption and emission occur within the glass cover plate. Further, since both $I(\mathbf{r},\mathbf{s})$ and T (in $I_b(\mathbf{r})$) appear in the RTE (Eq. 1) for the glass cover plate, the RTE must be solved simultaneously with the appropriate energy equations for all of the materials in the oven.

Boundary Conditions. At the opaque boundaries (oven walls and food surface), the radiative heat balance equation is obtained by combining the radiative surface energy balance and Kirchoff's law, i.e., absorptance equals emittance for zero transmittance. With the diffuse radiation assumption, the incident radiative heat flux, q_{in}, at a wall is

$$q_{\text{in}} = \int_{\mathbf{s}\cdot\mathbf{n}>0} I(\mathbf{r},\mathbf{s})\mathbf{s}\cdot\mathbf{n}d\Omega \tag{2}$$

where the integral is over all incident directions above the wall and $d\Omega$ is at differential solid angle. The net radiative flux, q_{out} leaving the surface is given by

$$q_{\text{out}} = (1-\varepsilon_w)q_{\text{in}} + n^2\int_0^\infty E_{\lambda,w}d\lambda \tag{3}$$

where ε_w is the surface emittance, n is the refractive index of the medium next to the surface, and $E_{\lambda,w}$ is the emission function for the surface. Note that a directional integral does not appear in Eq. 3 due to the diffuse approximation. The boundary radiant intensity for all outgoing directions at the surface is given by

$$I_0 = \frac{q_{\text{out}}}{\pi} \tag{4}$$

For the semi-transparent boundaries also, i.e., the cavity glass, the reflected and transmitted radiation are assumed to be diffuse. There is no absorption at the semi-transparent boundaries. The interfacial reflectance, r_{d}, at the smooth, semi-transparent boundaries is assumed to be independent of direction and is estimated with:[24]

$$r_{\text{d,a}} = 1 - \frac{(1-r_{\text{d,b}})}{n^2} \tag{5}$$

$$r_{\text{d,b}} = \frac{1}{2} + \frac{(3n+1)(n-1)}{6(n+1)^2} + \frac{n^2(n^2-1)^2}{(n^2+1)^3}\ln\left(\frac{n-1}{n+1}\right) - \frac{2n^3(n^2+2n-1)}{(n^2+1)(n^4-1)} + \frac{8n^4(n^4+1)}{(n^2+1)(n^4-1)^2}\ln(n) \tag{6}$$

where $n = n_{\text{a}}/n_{\text{b}} > 1$ and a and b denote the two media bounding the semitransparent surface.

The radiant flux emitted by the halogen lamps is assumed to emerge as a diffuse heat source emission from two thin strips (representing the lamps, Figure 1) at the top surface of the cavity containing the lamps (see also the Section on Time Varying Boundary Condition for the Infrared Source).

Nongray Radiative Exchange. In the present study, to describe the effects of non-gray radiation, we divide the radiation spectrum into four wavelength bands as shown in Figure 3: 550–850 nm; 850–1350 nm; 1350–4250 nm; and beyond 4250 nm. We assume constant optical properties in each band. The reason for choosing the four wavelength bands is as follows: the source lamps emit primarily in the range 550–850 nm (Figure 2); potato emittance (the food studied) changes at 1350 nm (Figure 4); and the absorption coefficient of the glass changes at 4250 nm[20]; thus justifying the band cuts at these wavelengths. The radiation intensity per unit wavelength interval, I_λ $(\mathbf{r},\mathbf{s})$, is solved in each wavelength band:

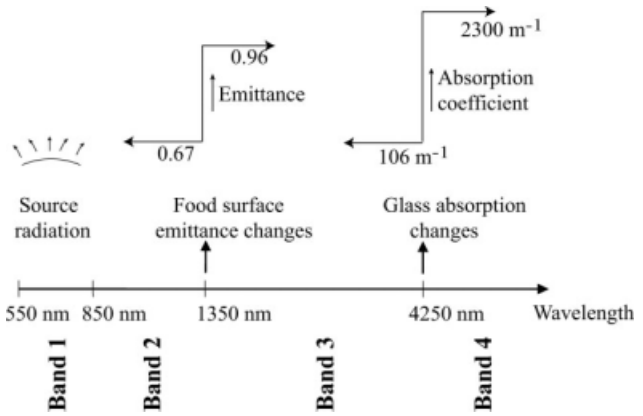

Figure 3. Division of the spectrum into gray bands as used in the model, following source, food, and cavity glass characteristics.

$$\nabla.(I_\lambda(\mathbf{r},\mathbf{s})\mathbf{s}) = -a_\lambda(I_\lambda(\mathbf{r},\mathbf{s}) + n^2 I_{b\lambda}(\mathbf{r})) \tag{7}$$

Equation 7 is integrated over each wavelength interval, resulting in transport equations for the quantity $I_\lambda\,\Delta\lambda$, the radiant energy contained in the wavelength band $\Delta\lambda$. The behavior within each band is assumed to be gray. The blackbody emission in the wavelength band per unit solid angle is written as

$$[F_{(0\to n\lambda_2 T)} - F_{(0\to n\lambda_1 T)}]n^2\frac{\sigma T^4}{\pi} \tag{8}$$

where σ if the Stefan-Boltzmann constant and $F_{(0\,\to\,n\lambda T)}$ is the fraction of radiant energy emitted by a black body in the wavelength interval from 0 to λ at temperature T in a medium of refractive index n and λ_2 and λ_1 are the wavelength boundaries of the band. The total intensity, $I(\mathbf{r},\mathbf{s})$, in each direction $\mathbf{s}$ at position $\mathbf{r}$ is computed using

$$I(\mathbf{r},\mathbf{s}) = \sum_k I_{\lambda_k}(\mathbf{r},\mathbf{s})\Delta\lambda_k \tag{9}$$

where the summation is over the wavelength bands.

Governing equations and boundary conditions for heat conduction

The energy equation (Eq. 10) is solved for the entire cavity (food, glass and air):

$$\rho c_p\frac{\partial T}{\partial t} + \rho c_p(\mathbf{u}.\nabla T) = k\nabla^2 T + Q\begin{cases} = 0 & \text{food, air} \\ = (\nabla.\mathbf{q_r} - an^2 I_b(\mathbf{r})) & \text{glass} \end{cases} \tag{10}$$

The density (ρ), specific heat (c_p) and the thermal conductivity (k) are evaluated for food, glass, and air, as appropriate. The maximum increase in the food-surface temperature is observed to be $\sim$35°C during the heating duration considered (Figure 10). The food properties are not expected to change by more than 5% in this temperature range. Therefore, physical properties of the food are assumed to be constant (Table 1). The volumetric heat source term, Q, is nonzero only in the glass. The heat source term is equal to the energy absorbed by the glass, $\nabla.\mathbf{q_r}$, minus the energy emitted by the glass, $an^2\,I_b\,(\mathbf{r})$. The radiative heat flux, $\mathbf{q_r}$ is given by:

$$\mathbf{q_r} = \sum_k\left(\int_0^{4\pi} I_{\lambda_k}(\mathbf{r},\mathbf{s})\mathbf{s}d\Omega\right)\Delta\lambda_k \tag{11}$$

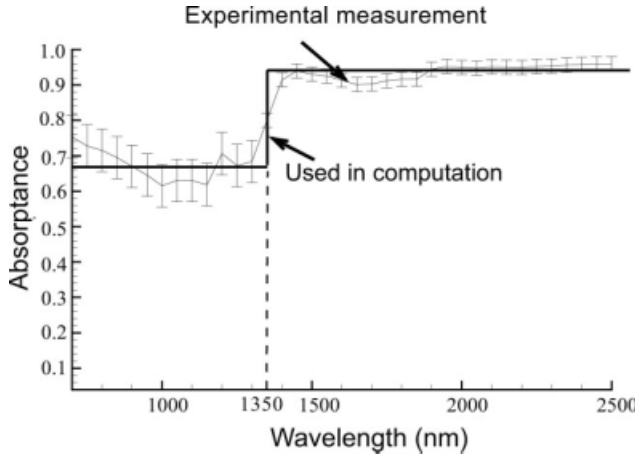

Figure 4. Measured spectral absorptance of potatoes in the near and mid-infrared range from[27] and the approximation (solid line) used in this study.

Table 1. Input Parameters Used in Simulations

Parameter	Value	Source
Air density	1.1614 kg/m^3	Bejan, 1993[26]
Air specific heat	1030 J/kg·K	Bejan, 1993[26]
Air thermal conductivity	0.045 W/m·K	Bejan, 1993[26]
Potato density	1000 kg/m^3	Talburt and Smith, 1959[27]
Potato specific heat	3900 J/kg·K	Talburt and Smith, 1959[27]
Potato thermal conductivity	0.4 W/m·K	Talburt and Smith, 1959[27]
Potato emittance (nongray) $\leq$ 1350 nm	0.67	Figure 4 (Almeida, 2004[25])
Potato emittance (nongray) $\geq$ 1350 nm	0.96	Figure 4 (Almeida, 2004[25])
Bulb cavity glass density	2650 kg/m^3	Wolfe, 1965[20]
Bulb cavity glass specific heat	786 J/kg·K	Wolfe, 1965[20]
Bulb cavity glass thermal conductivity	8.4 W/m·K	Wolfe, 1965[20]
Oven surfaces emittance	0.1	Gubareff et al., 1960[28]
Glass absorption coefficient $\leq$ 4250 nm	106 m^{-1}	Wolfe, 1965[20]
Glass absorption coefficient $\geq$ 4250 nm	2300 m^{-1}	Wolfe, 1965[20]
Bulb maximum output power	3 Kw	GE Advantium™ Specifications
Radiation temperature of the bulbs	4198 K	Measured

The velocity, **u**, is zero everywhere except in the lamp cavity. As noted, the ambient air is assumed to be radiatively nonabsorbing, i.e., non-participating. The thermal boundary condition on all solid surfaces for the energy equation (Eq. 10) is as follows:

$$\underbrace{-k_c \left.\frac{\partial T}{\partial n}\right|_c}_{\substack{\text{conduction from} \\ \text{solid to surface}}} - \underbrace{\left(-k_{air} \left.\frac{\partial T}{\partial n}\right|_{air}\right)}_{\substack{\text{conduction from} \\ \text{surface to air}}} = q_{out} + h_c(T_s - T_{air}) \quad (12)$$

where k_c is the thermal conductivity of the solid, k_{air} is the thermal conductivity of the air, n is the outward normal direction to the solid surface, q_{out} is the net radiative flux leaving the solid surface as given by the radiative boundary condition equation (Eq. 3). and h_c is a pseudo-convective heat transfer coefficient (more to follow). According to the user's manual for the oven, the lamp cavities are cooled by multiple fans (illustrated in Figure 1). It is not possible to measure the air velocity inside the lamp cavities without disturbing the system. Therefore, a sensitivity study of the glass temperature with respect to air velocity in the lamp cavities was carried out; hereafter, the value of velocity (and thus h_c) which gave the best estimate of the glass temperature (as compared to measurements) was used (discussed later in Results). This velocity is used in the estimation of the heat transfer coefficient, h_c, over the glass surface inside the lamp cavities, and which accounts for the effect of cooling due to forced convection.

The air in the main oven cavity is assumed to be quiescent and, thus, all walls have a zero heat transfer coefficient (natural convection is ignored). The two terms on the left side of the heat balance in equation (Eq. 12) represent conduction from within the solid to the solid surface, and from the solid surface to the surrounding air, respectively. In order to avoid the complications involved in modeling the oven wall thickness as well as insulation, it is assumed that no heat escapes from the oven cavities. Also, the heat capacity of the walls is assumed to be small. These assumptions are justified considering that the oven walls are made up of thin stainless steel sheets and the cavity is enclosed in a thick insulation material. Since the oven walls are adiabatic, the first term in equation (Eq. 12) is set to zero at those walls. For the food surface, this term is calculated using the heat conduction equation (Eq. 10) inside the food.

Input parameters

Table 1 lists the input parameters used for the simulations. The oven surface emittances are taken as those of stainless steel at 300 K. The potato emittance is set for two different values – 0.67 up to 1350 nm and 0.96 for wavelengths beyond 1350 nm, for the 4-band non-gray analysis described earlier. The emittance of the heat source is parametrically varied in time to describe the time cycling of the lamps (see discussion in the following paragraph). Quartz glass properties are used for the plate covering the bulb cavity.[20] The glass has absorption coefficients of 106 m^{-1} and 2300 m^{-1} for wavelengths below and above 4250 nm, respectively. For the 3.25 mm glass cover plate thickness, using the Beer-Lambert law, these values translate to absorption values of 29 % and 99 % for wavelengths below and above 4250 nm.

Time-Varying Boundary Condition for the Infrared Source. The halogen lamps that provide infrared energy to the oven cycle on and off, producing a time-varying heat flux. Only the heat flux due to the two halogen bulbs located in the oven ceiling is considered here. The radiation spectrum from the lamps was analysed using a high resolution fiber optic spectrometer, HR4000 (Ocean Optics Inc., Dunedin, FL). Figure 2 shows the intensity vs. wavelength obtained from the spectrometer and normalized with respect to the intensity at 690 nm, the wavelength corresponding to the peak. The maximum energy emitted by the lamps per unit time is assumed to be equal to the rated power of the top lamps, i.e., 1.5 kW each. This maximum power is then multiplied by a time function, $f(t)$, with values ranging from 0 to 1, to represent the transient behavior of the lamp. The function, $f(t)$, is found by measuring the radiation intensity at 690 nm versus time, and normalizing as noted in the foregoing. Figure 5 shows the $f(t)$ curves obtained in this way for the three power levels (settings on the oven dial) of I, V and X. The time function, $f(t)$, increases as the lamps are turned on and decays as the lamps are turned off.

The output energy emitted per unit time, $P(t)$, is related to $f(t)$ by

$$P(t) = 3000\, f(t) \quad (13)$$

The radiation simulation assumes constant optical properties in each band and cannot handle a spectrum with different emittances at each wavelength. To make the model consistent with the actual radiation spectrum of the source lamps, the emitted energy spectrum from the lamps is approximated as follows. The source lamps are replaced by two non-gray strips, at the top wall of the upper lamp cavity,

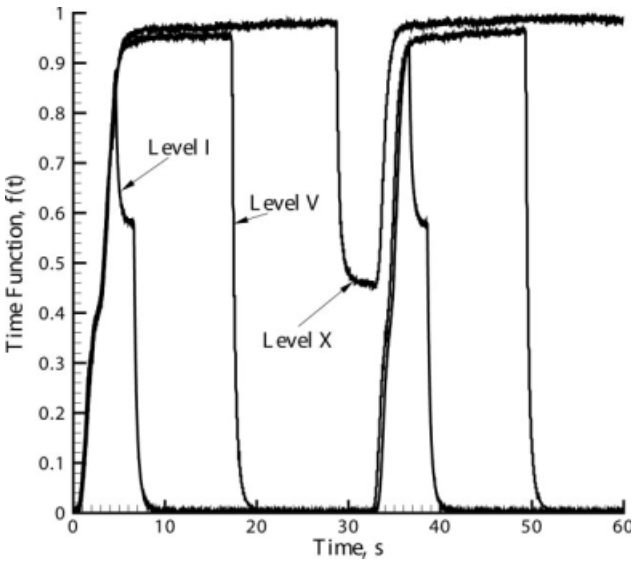

Figure 5. Time function, *f(t)*, in Eq. 13 for infrared power level settings I, V, and X.

The time function represents the radiation intensity at time t as a fraction of the peak intensity.

radiating at a fixed temperature, T_s of 4198 K (which matches the peak wavelength of 690 nm), and having a uniform non-zero emittance over the wavelength range 550-850 nm. The energy in this band was set equal to the measured (over all wavelengths) emitted energy. In Figure 2, the approximated spectrum (i.e., the band between 550 nm and 850 nm), is shown superimposed over the experimentally-measured spectrum. The emittance of the source, $\varepsilon_s(t)$, is then varied with time to represent the cycling of the lamps:

$$\varepsilon_s(t) = \frac{P(t)}{\sigma T_s^4 A_s F_{(0.85)(4198)-(0.55)(4198)\mu\text{mK}}} \tag{14}$$

The area of the two strips of the infrared source, A_s, is specified arbitrarily to be 40% of the area of the top wall of the upper cavity. Note that this arbitrary specification of area is done as only the product of emittance and area can be known and not their individual values. The change of area is not expected to significantly change the glass or food fluxes or temperatures, as the total emitted radiation energy and the spectrum remain the same regardless of the chosen area.

Convection Cooling over the Solid Surfaces. The duration of heating in this study is one minute. Natural convection airflows in the main oven cavity are induced with the start of heating and then relax to zero when the radiant heaters are shut off and the surfaces cool. Because of the high Rayleigh number ($>10^9$) beneath the lamp cavity glass, and because the associated boundary layer would develop in a density-stratified media, the modeling of the natural convection currents inside the main cavity would be a separate study in itself.[29] Although it is possible to estimate the steady-state, fully-developed heat transfer coefficients for a heated rectangular block and the walls inside a cavity,[30] it was shown elsewhere[25] that the oven takes several minutes to reach a convective steady-state condition. Thus, for a one minute heating period that includes lamp cycling over even shorter time intervals, a steady-state heat transfer coefficient (the value of 4.5 W/m^2 K) would not be appropriate. In this study, for simplification, we have ignored the cooling due to the natural convection of air adjacent to solid surfaces. However, the effect of forced convection cooling in the upper lamp cavity is accounted for by specifying a constant velocity of 12.5 m/s for the air in the cavity (as discussed under Governing Equations and Boundary Conditions for Heat Conduction).

Numerical solution

The radiative transport equation, RTE (Eq. 7), is approximated using the method of Discrete Ordinates (DO)[31] to handle directional effects and is solved numerically, together with the energy equation (Eq. 10), using FLUENT^{TM} 6.3.26, a commercial CFD software package. The RTE has direction as an independent variable, and thus direction is discretized as are the other independent variables, x,y and z. In the present study, each octant of the angular space was divided into 3 (polar) $\times$ 3 (azimuthal) control angles of equal extent. Thus, in all $8 \times 3 \times 3 = 72$ directions are solved for each band. Further details of the discretization are available elsewhere.[31]

For the energy equation, a hexahedral mesh was used with 381,786 cells. A second order upwind scheme was used for the x-y-z spatial discretization, while a first order implicit scheme was used for the time integration. Simulations were performed on an 8 node cluster of Dual Processor 3.6 GHz Xeon EM64T workstations with 4 GB RAM per node. The wall clock time for one second of simulation was about 30 min.

Experimental Measurements

The oven and the food system

As shown in Figure 1, the GE Advantium^{TM} oven (Model no. SCA2000BBB 03) is a combination oven with microwave and infrared (halogen) heating capabilities. It has three halogen lamps of 1.5 kW power each, inside two cavities – two lamps in the top cavity and one in the bottom. The top and bottom cavity lamps can be controlled independently. For the purpose of this study, only the top lamps were used so that experiments and simulation could be carefully compared. The oven has microwave heating as an additional heating mode,[25] but that mode was not used in the present study.

The dimensions of the main cavity of the oven are 0.470 m $\times$ 0.356 m $\times$ 0.215 m (Figure 1), with a volume of 0.036 m^3. All the inside surfaces, besides the lamp covers and the front window, are brushed stainless steel. The power levels of infrared heating are set through a dial on the oven control panel. The dial has 10 settings from I to X which determine the on-off cycle times for the halogen lamp. Larger numbers correspond to longer on-times. Heating duration can be adjusted in intervals of 15 s.

The food sample is a rectangular slab of potato (TOPS SELECT Golds brand), obtained from a local grocery store, and sliced into dimensions 1/10th that of the oven, 0.0470 m $\times$ 0.0356 m $\times$ 0.0215 m. The sides of a potato sample were aligned with the corresponding sides of the oven. The sample was placed 2.54 cm above the geometric center of the bottom surface of the oven. The food sample was stationary during the experiment and was initially at room temperature. A previous study[21] characterized the spectral radiative properties of the potato samples.

Temperature measurements on glass surface below top lamp

As illustrated in Figure 1, the temperature history of the underside of the glass surface was obtained using a K-type thermocouple (Omega Engineering, Stamford, CT), which has a sensitivity of 41 μV/°C, with $\pm$ 1.5°C uncertainty. The sensor was cemented onto the glass using high conductivity Omegatherm paste from the same company and was supported by paper tape. Temperatures were recorded every 1 s for three oven cyclic settings (namely, I, V and X), using the top lamps only.

Temperature and heat flux measurements on the food surface

Temperature and incident heat flux on the food surface were recorded using an Omega Thin Film Heat Flux Sensor

HFS-3 (Omega Engineering Inc., Stamford, CT). This thermocouple was cemented onto the surface using Omegatherm paste and paper tape. The heat flux in the differential thermocouple sensor is proportional to the temperature difference across the sensor, which is measured directly. The planar dimensions of the sensor are 35.1 mm $\times$ 28.5 mm, with long lead wire extensions for connections. The upper temperature limit for the sensor is 165°C. The HFS-3 is a precalibrated heat flux sensor, which gives a voltage as output with a sensitivity of 0.95 $\mu V/(W/m^2)$, with $\pm$ 10% uncertainty. The maximum recommended heat flux for the sensor is 94.6 kW/m^2, much larger than the fluxes encountered in this study. A K-type thermocouple is built into the heat flux sensor to record temperature.

The sensors are interfaced with a FLUKE Data Acquisition Bucket (FLUKE, WA) which directly measures the voltage with no need of cold-junction compensation. For the three oven infrared settings used in this study, heating was restricted to 1 min durations to minimize the effects of evaporation. A 1 min duration covers about two lamp cycles. The same data acquisition system was used for the glass cover temperature, the food temperature, and the food heat flux measurements.

Results and Discussion

Transient radiative exchange analyses were performed for one minute heating cycles of the lamps, as described in Time-Varying Boundary Condition for the Infrared Source, to obtain temperature and heat flux values on the food and glass surfaces. In this section, time step convergence and comparisons with experimental temperature and heat flux values are described. The effects of power level, gray versus non-gray treatments, and various food and wall emittances are examined.

Time step convergence

The significant computational effort involved in the simulation of a 3D, 4-gray band discrete ordinates radiation model, as discussed in Numerical Solution, requires the use of the largest possible time step for which the solution is still independent of time step size. Figure 6 shows the temperature at the mid-point of the lower surface of the upper lamp cavity for 15 s of heating time using different time step sizes. The temperature stops changing for time step sizes smaller than about 0.1 s, which is the step size used for all the simulations.

Glass temperatures

The glass that covers the upper cavity absorbs part of the radiation coming from the lamps and transmits the rest. In order to predict the food temperature and fluxes, it is essential to accurately account for the glass behavior. Figure 7 compares the experimentally-measured and numerically-simulated temperature histories at the geometric center of the bottom surface of the glass for all three power levels. For all three power levels, the glass temperature follows the time function, $f(t)$, as temperature rises initially. The temperature keeps on rising as $f(t)$ becomes flat at its peak value (both lamps switched on at full power) and starts decaying at a very slow rate after the lamps are switched off ($f(t) = 0$).

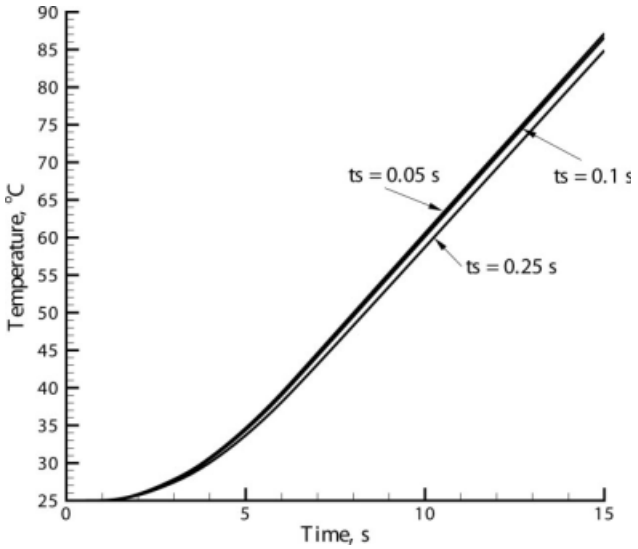

Figure 6. Temperature at the center position on the underside of the glass surface covering the top infrared lamps during 15 s of heating for three different time step sizes for infrared power level X.

Figure 8a shows numerically-calculated glass temperature contours at $t = 4s$ for power level I. We can see that the temperature is the highest in the regions directly below the lamps and is a strong function of the relative distance from the lamp strips. Also, at $t = 12s$, when the lamps are off and the source radiation is subsiding, the glass temperature spatially decreases from the end where the cooling air enters the lamp cavity to the end where the cooling air leaves. The effect of the cooling air in the lamp cavity is further illustrated in Figure 9, where the mid-point temperature for power level I is shown for three different assumed air velocities of 7.5 m/s, 12.5 m/s and 17.5 m/s. For a velocity of 7.5 m/s, the temperature is almost constant after the lamps are switched off. At higher values of velocity, while the peak temperature values are the same, the temperature starts to decrease after the lamps are switched off. Thus, it can be deduced that the cooling air and the relative position from the lamp are the primary factors affecting the glass temperature. These spatial gradients along with the transient nature of the lamp power, $f(t)$, make the comparison of glass temperatures difficult. Nevertheless, the good match demonstrated in Figure 9 at the mid-point of the glass plate for all three power levels supports the heat transfer model used for the upper lamp cavity. Note that the objective was to model the temperature history of the glass and not to characterize the flow inside the cavity. Therefore, simulations were run using different velocity values for the upper cavity air to find the best match; the best match was judged to occur for a velocity of 12.5 m/s.

Food fluxes and temperatures

The primary interests in this study are the temperature and heat flux at the food sample being heated. For validation,

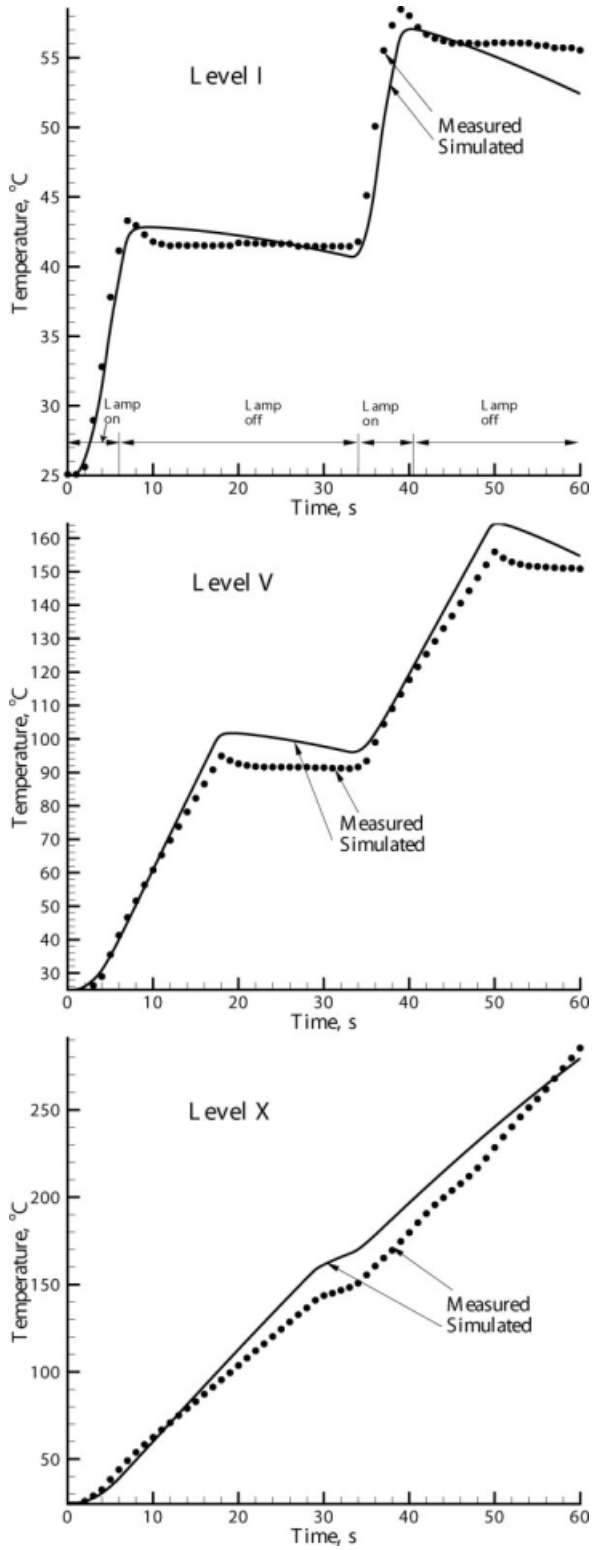

Figure 7. Experimental and computed temperatures at the center position on the underside of the glass surface covering the top infrared lamps during 1 min of heating for three different settings of infrared power level (Levels I, V, and X) in the Advantium™ oven.

Figure 10 compares the numerically-computed heat flux and temperature values, averaged over the region covered by the thermocouple sensor on the top of the food, with the experimentally measured values for three power levels. The fluxes follow the growth and decay transients of the lamp, as expected.

Temperature rises with the growth of lamp power and then decays at a slower rate. This decrease in temperature is due to heat loss to the surrounding air as well as heat conduction to the cooler interior regions of the food sample. Figure 11 shows temperature contours in the food sample at various cross-sections.

For the three power levels, the food surface temperature reaches peak values of 35°C, 52°C and 65°C, respectively. The model is able to predict the temperature and heat flux cycling reasonably well for the initial 30 seconds and longer. However, during the times when the lamps are off (from

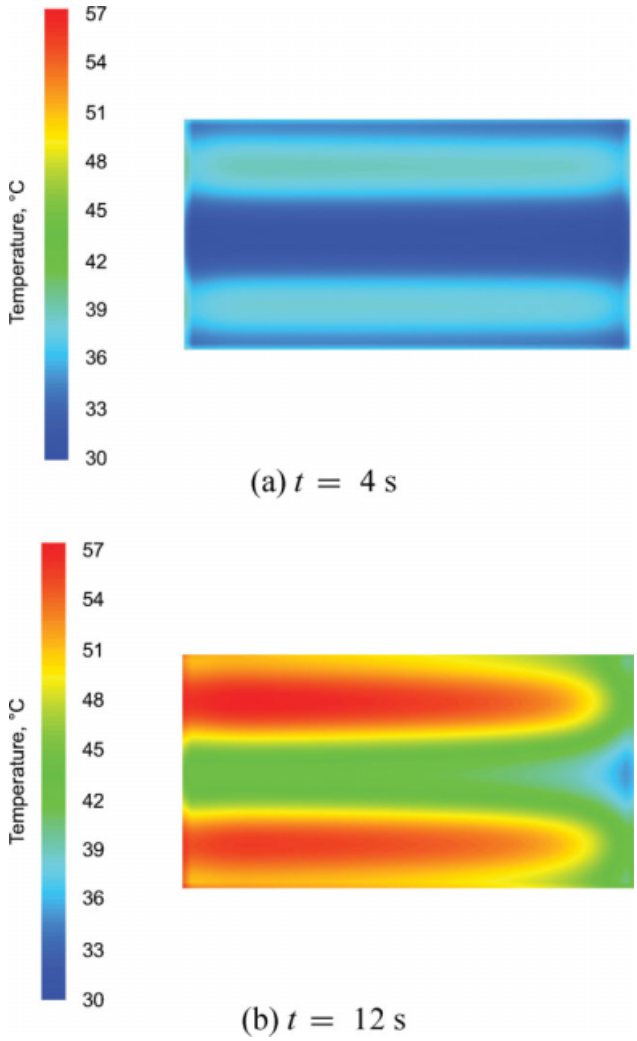

Figure 8. Calculated temperature contours on the underside of the glass surface covering the top infrared lamps at 4 s and 12 s for power level I.

[Color figure can be viewed in the online issue, which is available at www.interscience.wiley.com.]

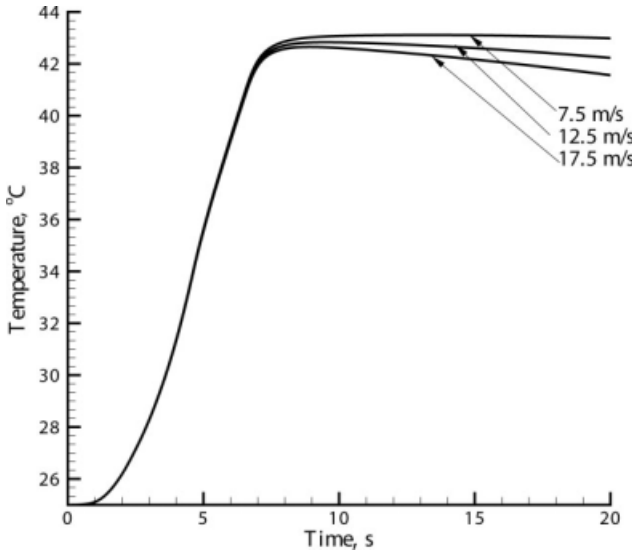

Figure 9. Calculated temperatures at the center position on the underside of the glass surface covering the top infrared lamps during 20 s of heating at power level I with three different values of air velocity in the upper lamp cavity.

7 to 34 s and from 41 to 60 s for level I heating; and from 17 to 34 s and from 51 to 60 s for level V heating), the cooling rates are underpredicted. This is most likely due to the neglect of surface evaporation and natural convection in this study (see Convection Cooling over Solid Surfaces) which cause the food surfaces to cool faster once the lamps are off. The effect of evaporative cooling becomes prominent at higher temperatures, especially in the level X temperature and heat flux histories (Figure 10c), when the heating rate is overpredicted. Even with these limitations, the error in food temperatures and heat fluxes is within 15% for most of the time for all power levels, which is a very good match, considering that the system is a commercial oven and not a laboratory experiment where all the parameters can be controlled.

One of the most interesting features elucidated by the present nongray radiation analysis is the band-wise distribution of energy absorbed by the food sample. Such information may provide insights as to where design efforts should be spent to improve the efficiency of the process. This information is critical while studying the kinetics of photochemical reactions occurring in the food, which lead to loss of food nutrients and formation of undesired free radicals.[2] Figure 12 shows the power absorbed by the food surface, in the four radition bands, over time for three power levels. Here, Band 1, i.e., from 550 nm to 850 nm wavelength, is the direct and wall reflected source-lamp radiation band. All the other bands correspond to radiation emitted by other sources, i.e. the oven walls and glass. It can be observed that indirect heating from the walls contributes significantly to the total power absorbed by the food, and constitutes more than 50% of the flux after the initial few seconds during which the oven walls and the glass are getting heated.

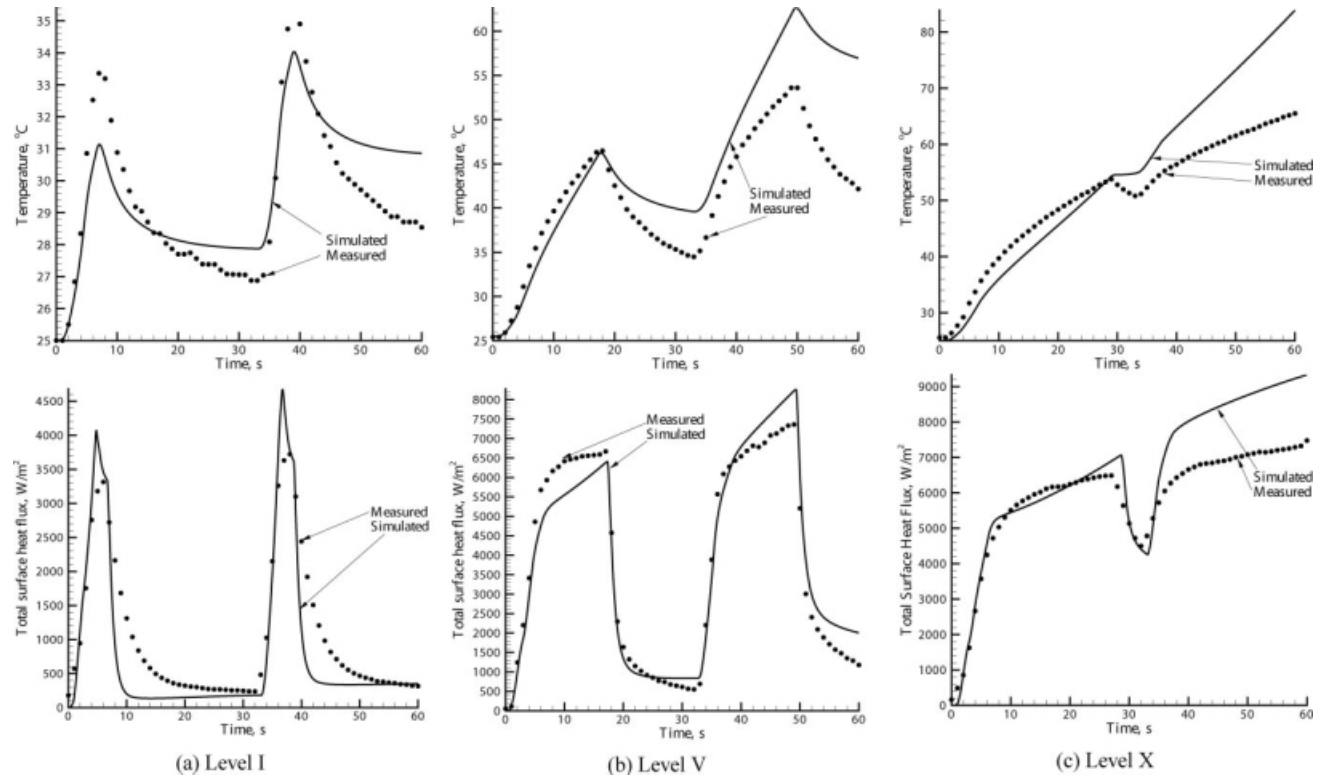

Figure 10. Experimental and computed temperatures and total surface heat fluxes at the center position on the top surface of the food during 1 min of heating for three different settings of infrared power level (Levels I, V, and X) in the Advantium™ oven.

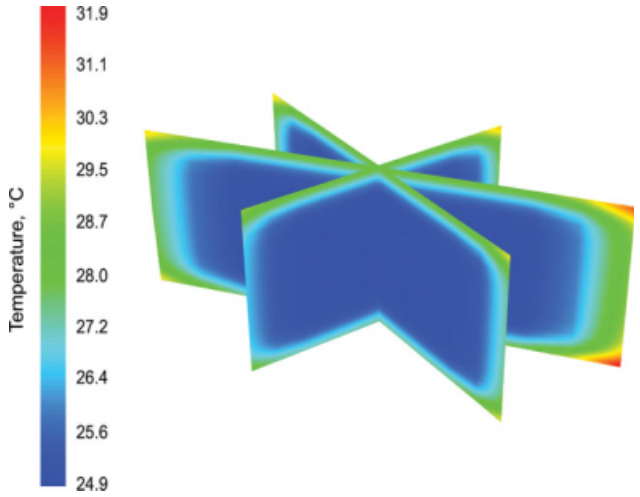

Figure 11. Temperature contours at different cross-sections of food at t = 12 s for power level I.

[Color figure can be viewed in the online issue, which is available at www.interscience.wiley.com.]

The energy efficiency of the process, i.e., the ratio of the energy absorbed by the food to the total input energy can be an important factor when designing an oven. Considering 3 kW as the input energy, the fraction of energy delivered to the food over its entire surface at the peak of lamp power emission was estimated to be around 0.8, 1.2, and 1.5%, respectively, for power levels I, V, and X. Such small values are probably due to the small size of the food sample. It would be useful to compare these numbers for different food sizes; however, such a study was beyond the scope of the current project due to the large computational resources required for each simulation. Future work could also consider various combinations of the three possible heating modes: infrared, convection and microwave.

Effect of food surface emittance (Gray vs. Nongray)

Measured data for the potato surface exhibit non-gray behavior as shown in Figure 4, where the emittance is 0.67 for wavelengths < 1350 nm and 0.96 for wavelengths > 4250 nm.[25] These values were used in this study. Typically, however, only wavelength-averaged emittance values are available for foods. The wavelength averaging is defined by:

$$\varepsilon_{\text{avg}} = \frac{1}{\sigma T^4} \int_0^\infty E_\lambda d\lambda \tag{15}$$

Averaging is only accurate when all the radiation sources have identical temperatures. When surfaces at different temperatures are present (e.g., source lamps, glass, and oven walls in the current study), the use of such an average may not be appropriate.

We carried out a brief study of gray versus nongray food emittance. Simulations (for power level X) were carried out for three different food surface emittance combinations: 0.67 for all wavelengths; non-gray surface (0.67 for wavelengths < 1350 nm and 0.96 for wavelengths > 4250 nm); and 0.96 for all wavelengths. Calculated temperature and heat flux profiles at the center of the top surface of the food sample are shown in Figure 13. Early in the transients, the flux and temperature profiles for $\varepsilon_{\text{food}} = 0.67$, which is gray, and the nongray case nearly coincide. This is because almost all the heat coming to the food is from the source lamp, i.e., with wavelengths < 1350 nm, for which $\varepsilon_{\text{food}}$ in both the cases is 0.67. However, as the oven walls get heated and start

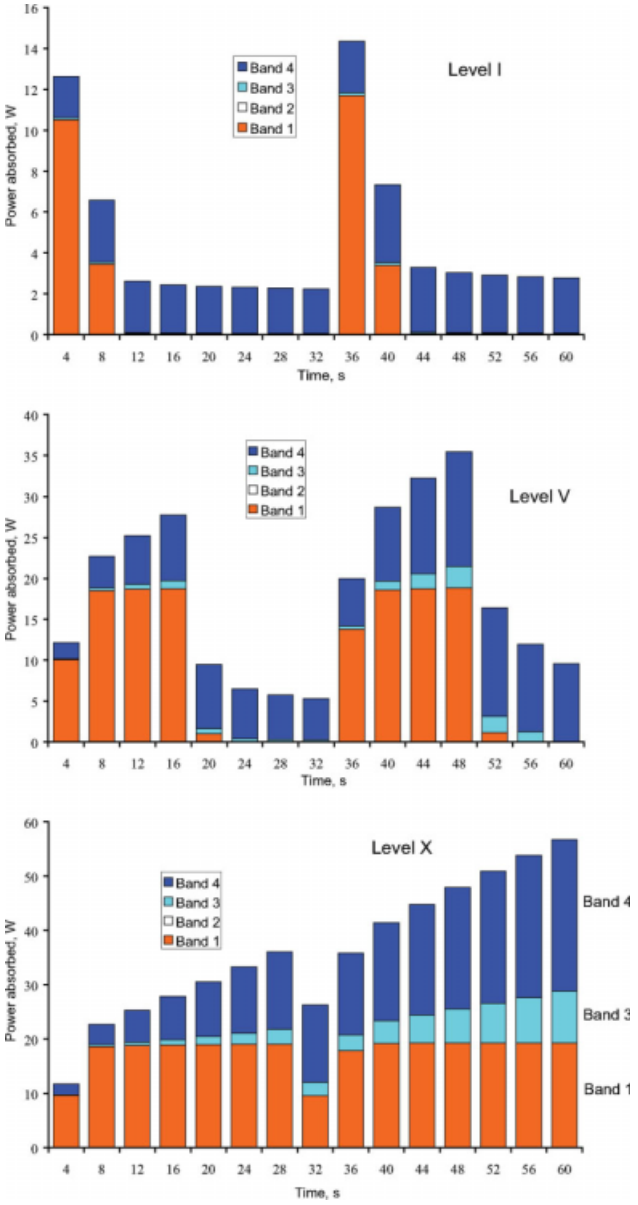

Figure 12. Distribution of the total power absorbed by the food in four radiation bands over time for power levels I, V, and X.

Bands are defined in Figure 3. The contribution from Band 2 is negligible for all three power levels at all times. [Color figure can be viewed in the online issue, which is available at www.interscience.wiley.com.]

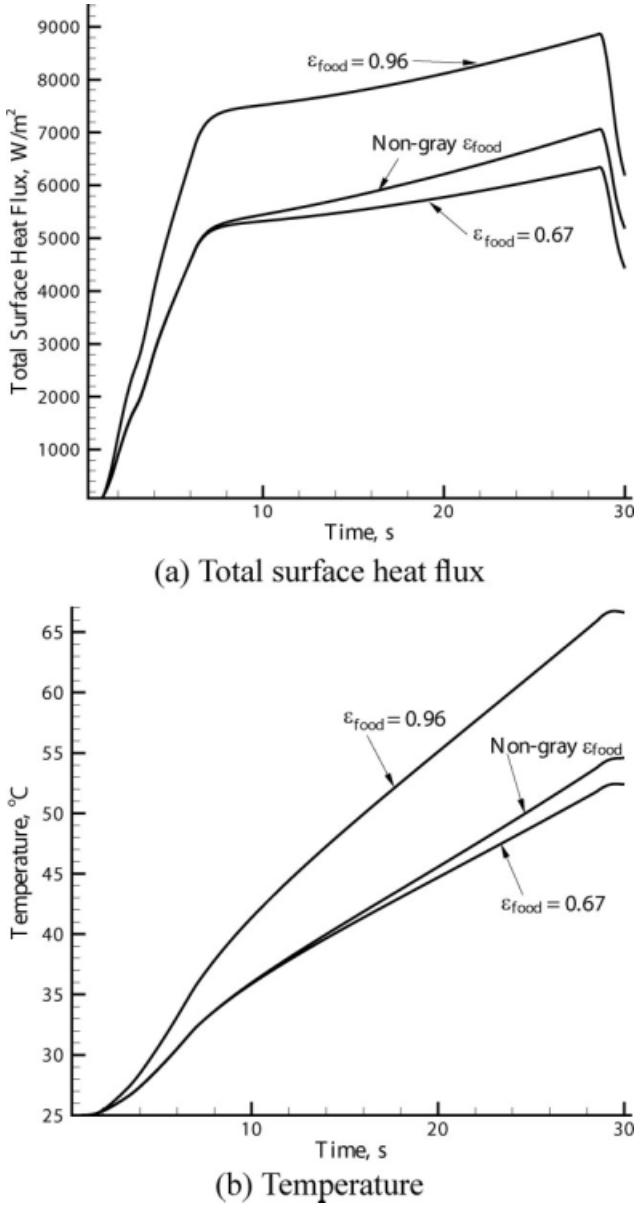

Figure 13. Experimental and computed temperatures and total surface heat fluxes at the center position on the top surface of the food during 30 s of heating for three different food surface emittance values for power level X.

contributing significantly to the heat delivered to the food, the profiles with $\varepsilon_{food} = 0.67$ start to fall below the nongray case. This is because the oven walls emit radiation with longer wavelengths, and for which the food emittance should be 0.96 and not 0.67. This effect will be much more pronounced at later times when emission from the oven walls becomes larger and also when the lamps are completely shut off and all the heating is provided by the oven walls. When used for the whole duration of heating, the $\varepsilon_{food} = 0.96$ value gives much larger food surface absorbed fluxes and temperatures for obvious reasons.

Effect of wall emittance

Oven walls reflect the source radiation and after getting heated, emission from the oven walls can be more than 50% of the total heat absorbed by the food sample (see Band 4 in Figure 12). Hence, it becomes important to know how the surface properties of an oven can influence food heating. Figure 14 compares heat flux and temperature profiles for two different oven wall emittance values, 0.1 and 0.05, for power level X for 30 s of heating. This emittance range brackets the range for clean stainless steel.[28] For the lower wall emittance value, the fluxes and temperatures at the food

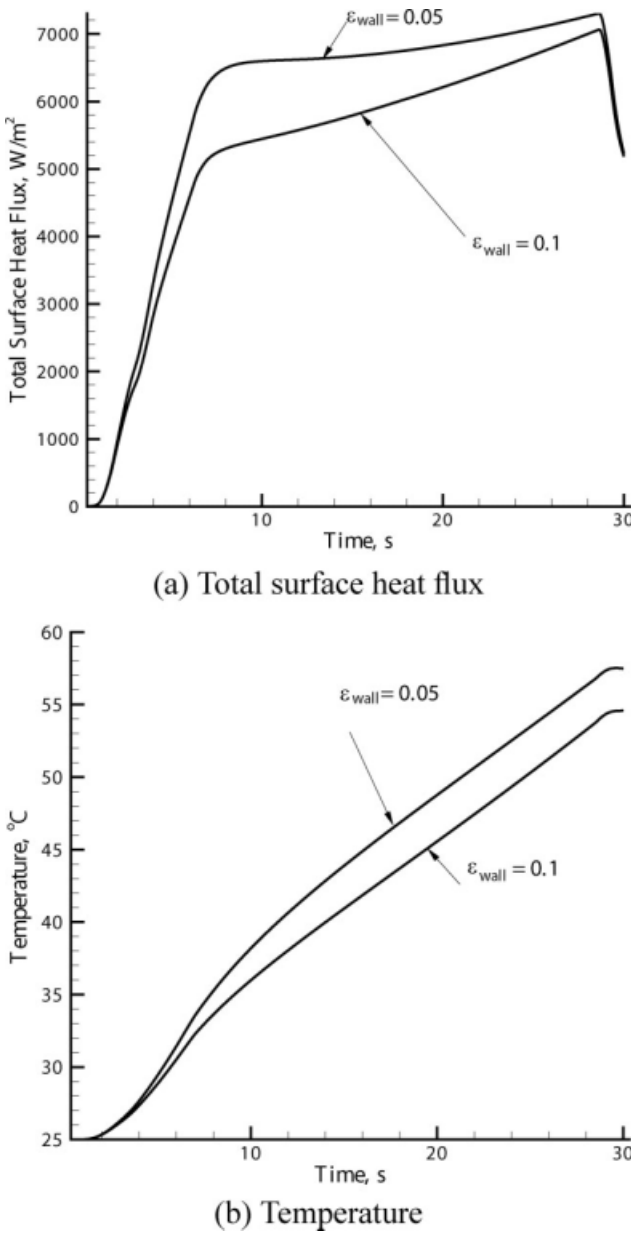

Figure 14. Experimental and computed temperatures and total surface heat fluxes at the center position on the top surface of the food during 30 s of heating for two different oven wall emittance values for power level X.

are higher by around 30% and 15%, respectively, after 8 s of heating because of greater reflection by the walls to the food surface. With time, the difference between the two flux values decreases as direct emission from the walls becomes significant and compensates to a certain extent for the lower reflectance of the $\varepsilon_{wall} = 0.1$ surface.

Conclusion

A 3D, 4-band, nongray radiation model was developed which can predict heat transfer inside an oven cavity. The total energy delivered to a food sample was estimated and its distribution among the four wavelength bands was shown to change as heating progressed. The contribution of the oven wall emission was found to be more than 50% after the initial heating-up period. The effect of variation of the food surface emittance with wavelength on the heating process shows that a non-gray treatment is necessary due to the presence of radiation in different wavelength bands. The effect of wall emittance shows that lower emittance (and thus higher reflectance) leads to higher heating rates of the food. In addition to providing fundamental insights into the radiative heating process in an oven, the detailed model presented can be used to optimize various design parameters of an oven such as geometry of the cavity, cycling time, source and food placement and other oven arrangements, thus, reducing time and costs associated with trial and error experimentation.

Acknowledgements

This research was conducted using the resources of the Cornell University Center for Advanced Computing, which receives funding from Cornell University, New York State, the National Science Foundation, and other leading public agencies, foundations, and corporations. The authors also acknowledge ANSYS-Fluent for providing the software license.

Notation

a = absorption coefficient, m^{-1}
A = area, m^2
c_p = specific heat, J/kg K
$f(t)$ = fraction of total lamp power emitted at time t
E_λ = irradiance as a function of wavelength, W/m^2
$F_{(0-n\lambda_i T)}$ = band energy ratio
h_c = convective heat transfer coefficient, W/m^2 K
$I(\mathbf{r},\mathbf{s})$ = intensity of radiation at a location $\mathbf{r}$ in direction $\mathbf{s}$, W/m^2
$I_b(\mathbf{r})$ = blackbody emission at a location $\mathbf{r}$, W/m^2
I_0 = radiation intensity at a surface, W/m^2
k_c = thermal conductivity, W/m K
n = refractive index
$P(t)$ = power of the lamps at time t, W
q = heat flux, W/m^2
$\mathbf{r}$ = position vector
r_d = interfacial reflectivity at a surface
$\mathbf{s}$ = direction
T = temperature, K
t = time, s
$\mathbf{u}$ = velocity of air, m/s

Greek letters

ε = emittance
λ = wavelength, m
ρ = density, kg/m^3
σ = Stefan-Boltzmann's constant, 5.67×10^{-8} W/m^2 K^4
Ω = solid Angle, rad

Subscripts

air = surrounding air properties
avg = average
c = solid
in = incoming
out = outgoing
surf = surface
r = radiation
s = source
w = wall
λ = at given wavelength, or per unit wavelength

Literature Cited

1. De Matteis M (inventor), Moulinex SA (assignee). Electric Microwave Oven with Improved Energy Distribution. US patent 6, 002, 120, December 14, 1999.
2. Uzgiris EE, Ackerman JF, Lillquist RD (inventors), General Electric (assignee), Radiant Oven. US patent 6, 018, 146. January 25, 2000.
3. Lee K (inventor), LG Electronics Inc. (assignee). Microwave Oven Having Halogen Lamps. US patent 6, 172, 347, January 9, 2001.
4. Cook ER (inventor), Maytag Corporation (assignee). Combination high speed infrared and convection conveyor oven and method of using. US patent 6, 369, 360, April 9, 2002.
5. Farkas B, Lloyd B, Keener K (inventors), North Carolina State University (assignee). Dynamic radiant food preparation methods and systems. US patent 7, 307, 243. December 11, 2007.
6. Dagerskog M, Sorenfors P. A comparison between four different methods of frying meat patties. I. Heat transfer, yield and crust formation. *Lebensmittel-Wissenschaft u. Technol.* 1978;11:306–311.
7. Shibukawa S, Sugiyama K, Yano T. Effect of heat transfer by radiation and convection on browning of cookies. *J Food Sci.* 1989;54:621–624, 699.
8. Kathiravan K, Kaur K, Soojin J, Irudayaraj J, Demirci A. Infrared heating in food processing: an overview. *Compr Rev Food Sci Food Saf.* 2008;7:2–13.
9. Cenkowski S, Hong JT, Scanlon JG, Arntfield SD. Mathematical modeling of heat and mass transfer during continuous infrared micronization. *Dry Technol.* 2004;22:2255–2272.
10. Wang J, Sheng KC. Modeling of muti-layer far-infrared dryer. *Dry Technol.* 2004;22:809–820.
11. Tanaka F, Morita K, Iwasaki K, Verboven P, Scheerlinck N, Nicolai B. Monte Carlo simulation of far infrared radiation heat transfer: Theoretical approach. *J Food Process Eng.* 2006;29:349–361.
12. Meeso N, Nathakaranakule A, Madhiyanon T, Soponronnarit S. Modelling of far-infrared irradiation in paddy drying process. *J Food Eng.* 2007;78:1248–1258.
13. Tanaka F, Verboven P, Scheerlinck N, Morita K, Iwasaki K, Nicolai B. Investigation of far infrared radiation heating as an alternative technique for surface decontamination of strawberry. *J Food Eng.* 2007;79:445–452.
14. Sato H, Hatae K, Shimada A. Effect of heating system on the evaporation process of food: Radiation and convection. *J Jpn Soc Food Sci and Technol (Nippon Shokuhin Kagaku Kogaku Kaishi).* 1999;46:508–513.
15. Skjoldebrand C, Andersson C. A comparison of infrared bread baking and conventional baking. *J Microwave Power Electromagn Energy.* 1989;24:70–75.
16. Franca FHR, Ezekoye OA, Howell JR. Inverse boundary design combining radiation and convection heat transfer. *J Heat Transf.* 2001;123:884–891.
17. Adams BR, Smith PJ. Three dimensionally discrete ordinates modeling of radiative transfer in a geometrically complex furnace. *Combust Sci Technol.* 1993;88:293–308.
18. Peterson M, Stenstrom S. Modeling of an electric infrared heater at transient conditions. Part I. Model and validation. *Int J Heat Mass Transf.* 2000;43:1209–1222.
19. Ojala KT, Lampinen MJ. Modeling, measurements and efficiencies of infrared dryers for paper drying. In: A.S. Mujumdar, editor. *Handbook of Industrial Drying*, Volume 2. New York: Marcel Dekker, 1995;931–976.

20. Wolfe WL. *Handbook of Military Infrared Technology*. Washington: Office of Naval Research, Department of the Navy, USGPO, 1965.
21. Almeida MF, Torrance KE, Datta AK. Measurement of optical properties of foods in near-and mid-infrared radiation. *Int J Food Properties*. 2006;9:651–664.
22. Raithby GD, Chui,EH. A finite-volume method for predicting a radiant-heat transfer in enclosures with participating media. *J Heat Transf*. 1990;112:415–423.
23. Siegel R, Howell JR. *Thermal Radiation Heat Transfer*, *4th ed*. New York: Taylor and Francis, 2001.
24. Siegel R, Spuckler CM. Effects of refractive-index and diffuse or specular boundaries on a radiating isothermal layer. *J Heat Transf*. 1994;116:787–790.
25. Almeida MF. Modeling Infrared and Combination Infrared-Microwave Heating of Foods in an Oven. PhD thesis. Cornell University, Ithaca, 2005.
26. Bejan A. *Heat Transfer*. New York: John Wiley & Sons, 1993.
27. Talburt WF, Smith O. *Potato Processing*. Westport, Connecticut: The Avi Publishing Co, 1959.
28. Gubareff GG, Janssen JE, Torborg RH. Thermal Radiation Properties Survey — A review of the literature. Honeywell Research Center, Minneapolis – Honeywell Regulator Company, Meneapolis, 1960.
29. Xamán J, Arce J, Álvarez G, Chávez Y. Laminar and turbulent natural convection combined with surface thermal radiation in a square cavity with a glass wall. *Int J Therm Sci*. 2008;47:1630–1638.
30. Sparrow EM, Abraham JP, Heat transfer coefficients and other performance parameters for variously positioned and supported thermal loads in ovens with/without water-filled or empty blockages. *Int J Heat Mass Transf*. 2002;45:3597–3607.
31. Murthy JY, Mathur SR. Radiative heat transfer in axisymmetric geometries using an unstructured finite-volume method. *Numer Heat Transfer Part B-Fundam*. 1998;33:397–416.

Manuscript received Sept. 12, 2008, and revision received Mar. 4, 2009.